A Wearable Upper Extremity Rehabilitation Device for Inducing Arm Swing in Gait Training

Jacob Bloom, Mohsen Alizadeh Noghani, and Babak Hejrati[1]

***Abstract*— This paper presents the design and validation of a proof-of-concept prototype for a wearable rehabilitation device to incorporate arm swing during gait rehabilitation. Unlike current stationary exoskeletons used for rehabilitation of upper limbs' function, assisting arm swing during gait requires inducing faster arm flexion/extension movements while maintaining the users' arms unconstrained in other directions. We developed a portable and underactuated system with features such as a large workspace and backdrivability to induce arm swing. Its wide workspace allowed the wearers to easily move their arms in different directions without any constraints. A modified double parallelogram linkage (mDPL) is proposed to allow the device to mimic the natural workspace of an arm. Additionally, a pulley drive and weight compensation system were created to place the motor on the users' back reducing the hindering weight of the actuators on their arms. Our experiments demonstrated this arm-swing rehabilitator could successfully induce arm movements at different arm configurations with low (0.67 Hz) and high (1.1 Hz) frequencies corresponding to slow and fast walking.**

2023 International Conference on Rehabilitation Robotics (ICORR) | 979-8-3503-4275-8/23/$31.00 ©2023 IEEE | DOI: 10.1109/ICORR58425.2023.10304737

I. INTRODUCTION

Arm swing is an essential part of human locomotion that increases rotational stability, balance, and energy efficiency during walking [1]. Gait rehabilitation often focuses on the legs and overlooks the role of the upper limbs, however, many patients do not demonstrate proper arm-swing patterns [2]. The upper limbs' muscle activity can also evoke more muscle activity in lower limbs due to interlimb neural coupling and, thereby, including arm swing can contribute to walking improvements of individuals with walking impairments [3], [4]. To maximize the effects of training, it is crucial for the patients to practice correct arm movements with proper coordination with the legs and sufficient amplitude [5]. Current methods, which aim to include arm movements in training, are often too simplistic and may result in undesired effects. The major shortcoming associated with the mentioned methods is the way the patients use their hands for interacting with these devices, which may lead to body weight compensation through hands that can lead to the learning of incorrect gait patterns [6].

The majority of currently existing upper extremity robotic devices are grounded and stationary exoskeletons that are designed for rehabilitation of upper limbs' function to improve the users' ability to perform activities of daily living [7], [8]. Such devices consist of multiple active degrees of freedom (DOFs) generating high assistive torques to produce relatively slow movements for training the users and helping them regain their upper limbs' ability. Assisting arm swing during gait, however, is a different task that requires inducing faster arm flexion/extension movements while maintaining the users' arms unconstrained in other directions. In addition to exoskeletons, research has shown that feedback systems can effectively induce and modulate different arm swing and gait characteristics to aid in rehabilitation [9], [10]. Although these studies demonstrate the potential of tactile feedback systems during rehabilitation to manipulate arm swing, such systems may not be suitable to instigate proper arm swing in individuals who are unable to demonstrate noticeable arm movements due to conditions such as stroke.

Given the importance of including arm swing for neurorehabilitation applications, this paper presents a novel design and a proof-of-concept prototype of an arm-swing rehabilitator for including arm swing in gait training. This novel device is as an assistive feedback system that is capable of performing harmonic motions to help induce and re-align arm swing. This device has the ability to assist the subject if they are not fully capable of performing the motion on their own. This paper presents a novel modified Double parallelogram linkage mechanism (mDPL) to increase the workspace of the proposed wearable device compared to the original DPL, which makes the system low-profile and allows the natural and unconstrained motion of the arms. This design is comprised of five passive DOFs enabling internal/external and abduction/adduction rotations as well as scapula motion while providing an active DOF for flexion/extension assistance. DPL reduces the complexity and obtrusiveness of the wearable and portable exoskeletons [11] compared to other designs such as a parallel-actuated mechanism [12], [13], a 3-DOF joint for glenohumeral shoulder rotation [14], and placing a passive joint directly at the humerus head [15]. Although soft robots satisfy ergonomic and workspace criteria [16], they are not suitable for inducing the high-frequency movements needed for our application.

For the virtue of users' ergonomics, it is crucial to remove unnecessary weights of the actuators from their arms. Therefore, this paper presents a design with a distally located actuator that utilizes a cable-driven system to transfer the motor's torque to the user's arm. Inspired by previous work [17], distally locating the motor on the user's back near T12 reduced the mass on the user's arm and improved the arm mobility. The developed cable-driven system for transferring the torques and power amplification enabled backdrivability and the execution of high-frequency motions.

*This work was supported by the National Science Foundation under Grant 2145177.

[1]Babak Hejrati (corresponding author) is with the Faculty of Mechanical Engineering, University of Maine, Orono, ME, US babak.hejrati@maine.edu

II. Design

A. The mDPL

To allow the wearer to perform internal and external shoulder movements, a modified double parallel linkage (mDPL) system was designed. The standard DPL forms a remote center of rotation about the humeral head of the user and will prevent any joint misalignment during internal/external rotation assuming the design is fitted to the anthropomorphic frame of the wearer. As demonstrated by Christensen et al. [11], a typical DPL rotates around a fixed center of rotation (CR), which enables it to cover the workspace of a shoulder joint. However, the fixed CR prevents the system from fitting to a wide range of shoulder types due to rotation about only a fixed radius which may cause joint misalignment. As shown in Fig. 1, the mDPL is comprised of two parallelograms (1-2-3-4 and 4-5-6-7) connected to each other at link 4. The proposed mechanism is capable of mimicking the same motions of a typical DPL, while allowing the CR of mDPL to be adjusted for each individual user resulting in a larger workspace. The adjustment of the CR is achieved by adding an extra translational degree of freedom to change the length of link 5 from its point of connection to link 7 (Fig. 1a-c) and, thereby, modifying the location of the CR if needed.

The mDPL was incorporated in the design of the arm swing rehabilitation device (Fig. 1d) to distally place the actuator, while enabling a wide fit and large workspace for its users. As shown in Fig. 2, the actuators are distally located at the user's back, and the mDPL is used to connect the motors to the user's upper extremities and transfer the generated torques to move the arms. Link 1 of the mDPL (Fig. 1) is connected to the system's backpack (Fig. 2c) and link 7 (Fig. 1) is connected to the user's arm. Figure 3 shows a prototype of the exoskeleton and the mDPL for the left arm, where the mechanism and main structural components of the device were 3D-printed. The wearable device comprises four passive and one active DOFs and is mounted on an ALICE backpack using a prismatic rail (Fig. 3b). This rail is used to help adjust the rehabilitator based on the user's shoulder width. The motor is distally located on the backpack instead of being directly (proximally) on the user's shoulder.

B. Pulley System

The torque from the distal motor is transferred to the arm through a pulley system, which also promotes the backdrivability of the device. Figure 4a shows the pulley system, in which the cables are directed along the inside of the mDPL via four constraint points (Fig. 4a). The constraint points allow the cable to move with the device while keeping them on the pulleys during motion as proposed in a previous study [17]. The cables are attached to the pulleys by crimping aluminum sleeves to the cable, and a pretension slide was added at the end of the mDPL linkage to adjust their tension. The inside of the pulleys uses a geometry that locks the crimped sleeves in place (Fig. 4b).

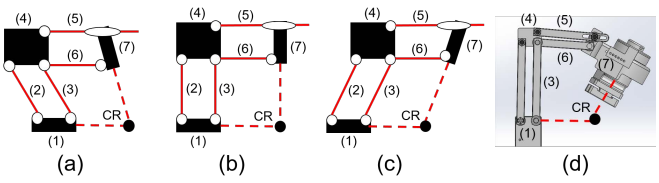

Fig. 1. The schematic drawing of the mDPL (top view) following the (a) external, (b) neutral, and (c) internal rotations of a shoulder as well as (d) the incorporation of the mDPL in the exoskeleton. In (a-c), the circles and ellipses represent rotary and prismatic joints, respectively

C. Ergonomics

The design for mounting the exoskeleton on the backpack enabled the compensation of the device's weight on the user's arm by the motor's weight. The device with the backpack weighs 6.08 kg (3.28 kg without the backpack), but the weight on the arm is only 0.9 kg. Therefore, the wearer feels only 27% of the device's weight on their arm. Another ergonomic characteristic of the device is the location of its center of mass. Using SolidWorks (Dassault Systems, MA, USA), the center of mass was approximated behind the wearer along the spine, which is associated with less discomfort when bearing a loaded backpack [17].

Two linear rails connect an arm brace (OR092-L, Or-

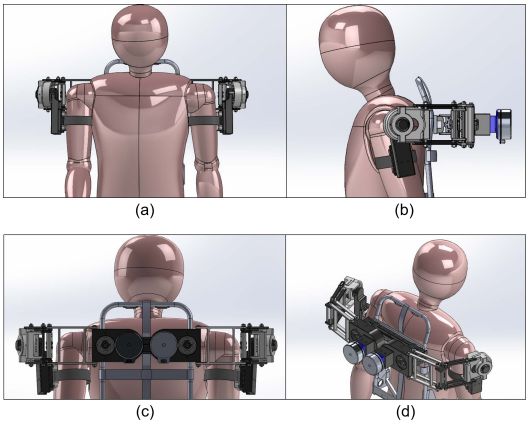

Fig. 2. A (a) front view, (b) side view, (c) back view, and (d) isometric view of a model wearing the device on both arms

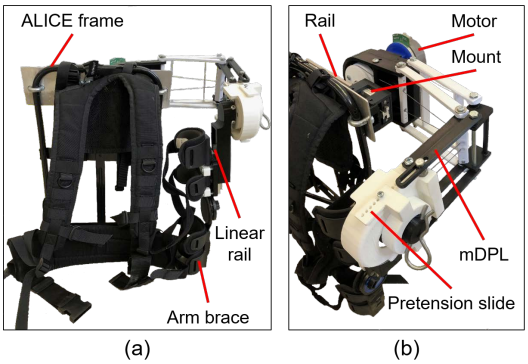

Fig. 3. The (a) front and (b) side-top views of the exoskeleton for one arm mounted on the backpack

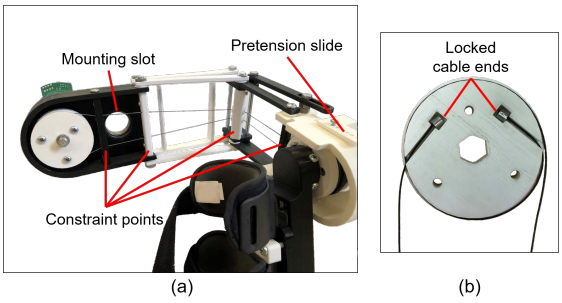

Fig. 4. (a) The pulley system of the arm swing rehabilitator and (b) the internal geometry of the shafts

thomen, CA, USA) on the user's arm to the mDPL. Using the arm brace along with the linear rails eliminates the kinematic constraint caused by the distance between the center of the user's shoulder joint and the system's center of rotation that can lock the movement of the arm [2] in the sagittal plane. Figure 5 shows that to avoid restricting arm movement, the distance from the CR of the exoskeleton (O_{exo}) to the connection point on the arm (O_c) needs to change. Figure 5a shows an arm in the neutral pose with the exoskeleton connected. There are three key points of O_s (CR of the shoulder), O_{exo} (CR of the exoskeleton), and O_c (connection point of the device to the arm brace). As the arm moves in either direction, the distances between O_s and O_c (a in Fig. 5) as well as O_s and O_{exo} (b in Fig. 5) remain constant. Therefore, to allow for arm movement, the distance between O_{exo} and O_c (d in Fig. 5) should be free to change by δ to $d \pm \delta$. Figure 5c compares the two triangles formed at the neutral and forward poses and shows a and b remain constant while the linear rails allow for d to change by δ.

D. Hardware and Electronics

The motor used was a Maxon (Maxon Precision Motors Inc., CH) EC 90 brushless motor attached to a 10:1 planetary gearbox (Vex Robotics, TX, USA). This provided up to 10 N-m of torque to the system. The motor was controlled using an EPOS4 driver (EPOS4 70/15, Maxon Precision Motors Inc., CH) and a Raspberry Pi 4 board (Raspberry Pi Foundation, UK). Using a custom code and EPOS Command Library, the Raspberry Pi sent position commands to the EPOS4 driver which then drove the motor to the desired position.

III. Forward Kinematics

Figure 6 shows the Denavit-Hartenberg (DH) coordinate systems of the device and the joints' axes of rotation for modeling the kinematics. The corresponding DH parameters are in Table I. For the exoskeleton, θ_1 is a passive degree of freedom that allows abduction and adduction of the arm. For forward kinematics calculations, the range of θ_1 was limited to $-90°$ to $0°$ to obtain the primary workspace of the device. θ_2, θ_3, and θ_4 are also passive DOFs of mDPL. Using the SolidWorks model to explore the range of θ_2, we found it to vary between -58° to 58°. As for θ_3, the maximum limit of the range always remained about -75.7°, but the lower

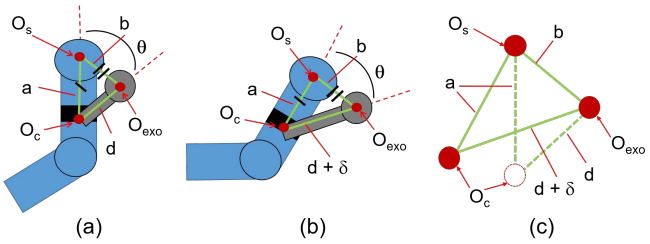

Fig. 5. The rehabilitation exoskeleton connected to (a) an arm at rest, (b) an arm performing flexion, and (c) the two resulting geometries of the shoulder and exoskeleton

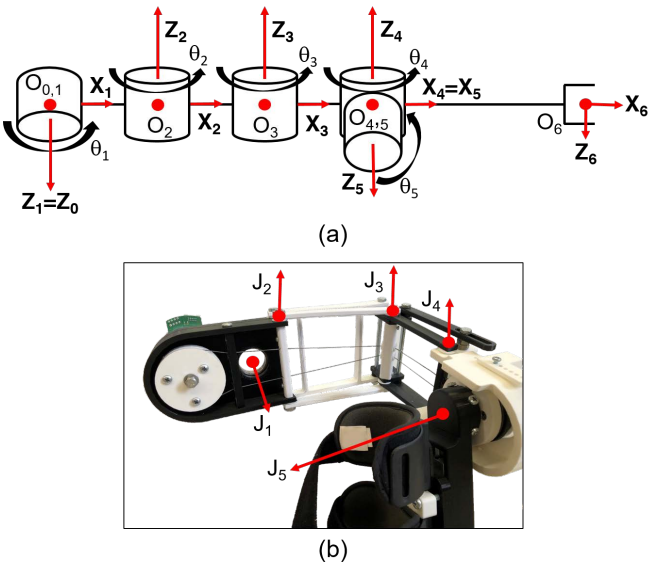

Fig. 6. A (a) zero-angle position (front view) of the device and (b) the labeled joints

TABLE I

DH PARAMETERS FOR THE DEVICE IN FIGURE 6; LENGTHS ARE IN M

i	a	d	α	θ
1	0	0	0	-90° $\leq \theta_1^* \leq$ 0°
2	0.04	0	-$\pi/2$	-58° $\leq \theta_2^* \leq$ 58°
3	0.15	0	0	$X_3 \leq \theta_3^* \leq$ -75.7°
4	0.10	0	0	θ_4^*
5	0.08	0	$\pi/2$	-140° $\leq \theta_5^* \leq$ 70°
6	0.16	0	0	-

limit (X_3 in Table I) depended on the value of θ_2 due to the kinematics of the mDPL that we found using SolidWorks. θ_4 does not affect the workspace of the device's end effector and is used to adjust the orientation of the brace on the arm ($\theta_4 \approx 0$). The last DOF is θ_5, which is actively controlled by the motor through the pulley system and is responsible for flexion and extension of the arm. The range of motion for this DOF is -140° to 70°.

Using the DH parameters in Table I, the forward kinematics for the device were solved to find homogeneous transformation, ${}^0d_{06}$ containing the end effector position expressed in the base frame.

$$ {}^{i-1}\mathbf{T}_i = \begin{bmatrix} \cos\theta_i & -\sin\theta_i & 0 & a_i \\ \sin\theta_i\cos\alpha_i & \cos\theta_i\cos\alpha_i & -\sin\alpha_i & -\sin\alpha_i d_i \\ \sin\theta_i\sin\alpha_i & \cos\theta_i\sin\alpha_i & \cos\alpha_i & \cos\alpha_i d_i \\ 0 & 0 & 0 & 1 \end{bmatrix} \quad (1) $$

$$ {}^{0}\mathbf{T}_6 = {}^{0}\mathbf{T}_1\,{}^{1}\mathbf{T}_2\,{}^{2}\mathbf{T}_3\,{}^{3}\mathbf{T}_4\,{}^{4}\mathbf{T}_5\,{}^{5}\mathbf{T}_6 \quad (2) $$

$$ {}^{0}\mathbf{T}_6 = \begin{bmatrix} {}^{0}\mathbf{R}_6 & {}^{0}d_{06} \\ 0^T & 1 \end{bmatrix} \quad (3) $$

where θ_i, α_i, and d_i are the DH parameters of the system, ${}^{i-1}\mathbf{T}_i$ is the homogeneous transformation between two adjacent frames, and ${}^{0}\mathbf{R}_6$ is the rotation matrix from the end effector to the base frame. The formula was evaluated in MATLAB for the joint space of the mechanism to obtain its workspace and exported to SolidWorks for visualization as shown in Fig. 7.

IV. Experimental

A. Inducing Arm Swing

To test the device's ability to generate arm swing, an experimental setup shown in Fig. 8a was created. The setup consisted of a 1 DOF shoulder joint that could rotate in a single plane similar to that of arm swing in the sagittal plane. The arm weighs 1.95 kg which is over half the weight of an average human arm and hand [18]. An Xsens IMU (Xsens Technologies B.V., The Netherlands) was placed on the arm and another on the motor shaft. The IMUs measured the respective angles of rotation at a sampling rate of 60 Hz. Two tests were conducted to induce: (1) in-plane and (2) out-of-plane arm swing, which can occur during the use of the device. The in-plane condition simulated arm swing when motion is strictly in the sagittal plane, while the out-of-plane condition simulated the case when the shoulder was internally rotated (25°) during arm swing (see Fig. 8b and c).

For both conditions, the motor rotated with an amplitude of ±25° at 0.67, 0.80, and 1.10 Hz, covering the frequencies of arm swing during natural walking [4]. A range of motion of 50° was tested because this is almost twice the range of motion of the shoulder during walking. The angles of the motor shaft and the arm were collected for 20 cycles. Cross correlations and time lags [19] were calculated to relate the motor's shaft angle to the angle of the passive arm. The range of motion of the arm was also compared between conditions. The maximum generated torque to move the passive arm during each trial was estimated using a simple one-DOF pendulum model using the measured angle θ and estimated angular acceleration $\ddot{\theta}$ of the arm. To validate that the device could also induce arm swing, the exoskeleton was tested on a human subject. The human subject had a height of 1.65 m and a shoulder width of 0.46 m. While wearing the device, the human subject was asked to keep their arm passively at their side and let the device move their arm in the direction of their natural arm swing with frequencies of 0.67 and 1.10 Hz.

B. Workspace Evaluation of the Rehabilitation Device

To demonstrate there was no kinematic lock on the natural motion of the user's arm, an experiment was performed to determine its workspace. A subject wore the exoskeleton and performed three trials that involved different movements while the system was not powered. The first movement was the flexion and extension of the arm. The second movement was the adduction and abduction of the arm. Finally, the subject performed internal and external rotations of the shoulder. We captured the range of motion of the arm in the frontal, sagittal, and transverse planes. To verify that the exoskeleton could be worn by users with different anthropometric sizes, three subjects wore the exoskeleton while it was not powered. This study was approved by the University of Maine's IRB. The subject's heights ranged from 1.65-1.83 m (1.75 ± 0.09 m), and their shoulder widths ranged from 0.42-0.46 m (0.44 ± 0.02 m). The subjects were asked to stand in their resting pose, perform a T-pose, perform an arm flexion, and reach across their bodies.

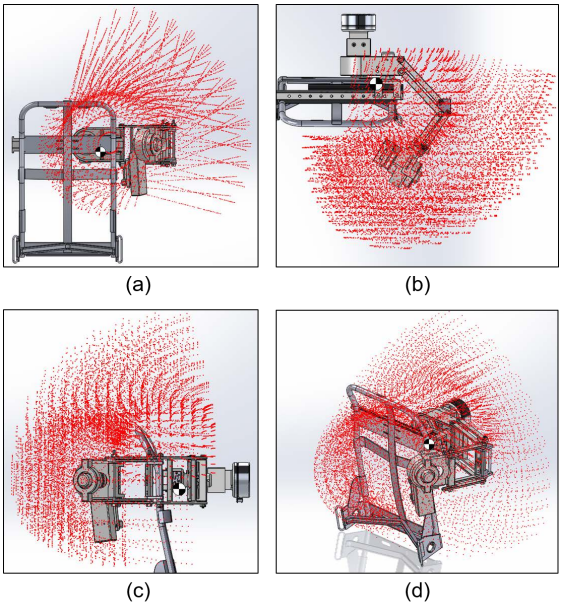

Fig. 7. Workspace of the exoskeleton and its center of mass as seen in the (a) frontal plane, (b) transverse plane, (c) sagittal plane, and (d) from an isotropic view

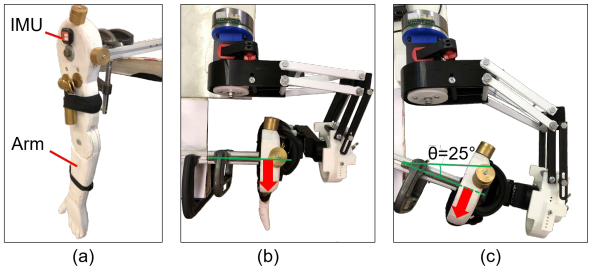

Fig. 8. The (a) passive arm (side view) in the (b) in-plane and (c) out-of-plane configurations (top views). The red arrows show the direction of arm swing. The angle in (c) shows the orientation of arm swing relative to the sagittal plane

V. Results

A. Inducing Arm Swing

Figure 9 shows the motor angle and the resulting passive arm angle across different frequencies and planes of motion conditions. The cross-correlations and time lags between the motor and arm angles are shown in Table II, and Table III presents the range of motion of the passive arm at each frequency. Figure 9a-b shows the device's response to an input frequency of 0.67 Hz. In the in-plane condition (Fig. 9a), a cross-correlation coefficient of -0.99 with a time lag of -0.03 s was observed between the two angles (Table II), while the range of motion of arm swing was 34.8° (Table III). Similar results were obtained for the out-of-plane condition at this frequency (Fig. 9b and Tables II and III). While the range of arm motion increased at the frequencies of 0.80 Hz and 1.10 Hz, cross-correlations and time lags were similar to those of 0.67 Hz, as reported in Table II. Table III shows shows the maximum computed torques during each trial. The generated torque increased with the frequency of arm swing, and the exoskeleton was capable of producing an estimated maximum torque of 7.19 N-m. The difference in torque between the two configurations was most pronounced in the low-frequency motion.

To evaluate the ability of the system to induce arm swing on a real human arm, the exoskeleton was tested on a human subject. The results showed high correlations between the arm and motor angles. The cross-correlation coefficients for 0.67 and 1.10 Hz were -0.98 (lag = 0.0167 s) and -0.93 (lag = 0.0167 s), respectively. The high correlations show the subject's arm quickly responded to inputs, and the device was capable of inducing arm swing at desired frequencies.

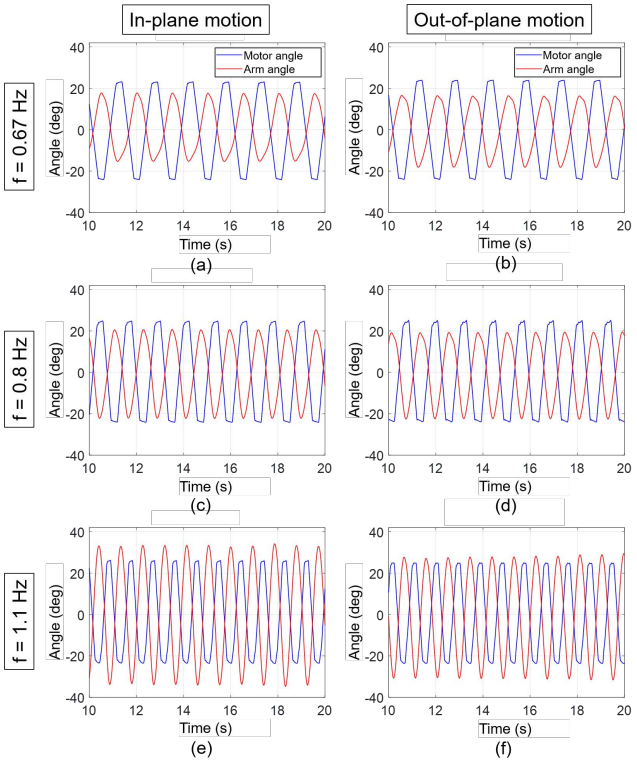

Fig. 9. Arm motion in-plane (first column) and out-of-plane (second column) at (a)(b) 0.67 Hz, (c)(d) 0.80 Hz, and 1.10 Hz (e)(f), respectively

B. Workspace Evaluation

Table IV shows the range of motion of a subject when wearing the exoskeleton. The ranges of motion of the device are compared to the anatomical limits of the shoulder joint as previously reported [11]. It should be noted that the limits are not attained during natural walking. To quantify the effect of wearing the rehabilitation device, the maximum angle in each direction of motion was compared to the human limits and reported as the percentage of coverage in Table IV. A more intuitive representation of the range of motion while wearing the exoskeleton is shown in Fig. 10, where the subjects with different sizes tried the system. Overall, it was observed that all the subjects could perform arm movement in different planes and directions without experiencing significant restrictions.

The flexion and extension movements of the arm swing device were limited using hard stops to prevent hyper-extension and hyper-flexion of the arm. Therefore, only 85% and 84% of the range for the flexion and extension of the arm, respectively, were covered. For abduction and adduction movements, the values of 171° and -64°, respectively, were achieved, confirming the device's ability to allow natural motions. The exoskeleton allowed for 33% of the external rotation normal range and 100% of the inter rotation. It should be noted the range of external rotation is sufficient given that here the goal is to mainly assist the arm's flexion and extension during walking.

VI. Conclusion

In this paper, a novel exoskeleton was presented for inducing arm swing to promote coordinated arm and leg movements during gait rehabilitation. A modified DPL was designed to create a wide workspace to accommodate the normal motion of the shoulder joint and arm. The device employed a distally located motor and a pulley system to avoid placing the actuator on the user's arm while enabling

TABLE II

Cross-correlation analysis between the movements of the motor and the passive arm

	In-plane		Out-of-Plane	
Frequency	**Cross-correlation**	**Time lag (s)**	**Cross-correlation**	**Time lag (s)**
0.67 Hz	-0.99	-0.03	-0.99	-0.02
0.80 Hz	-0.99	-0.02	-0.99	-0.03
1.10 Hz	-0.99	-0.05	-0.99	-0.05

TABLE III

Range of Motion and Computed Maximum Torque for the in-plane and out-of-plane passive arm

	Range of Motion		Generated Torque	
Frequency	**In-plane**	**Out-of-plane**	**In-plane**	**Out-of-plane**
0.67 Hz	34.8°	35.2°	2.65 N-m	3.19 N-m
0.80 Hz	43.7°	43.6°	4.38 N-m	4.53 N-m
1.10 Hz	69.6°	63.2°	7.19 N-m	6.87 N-m

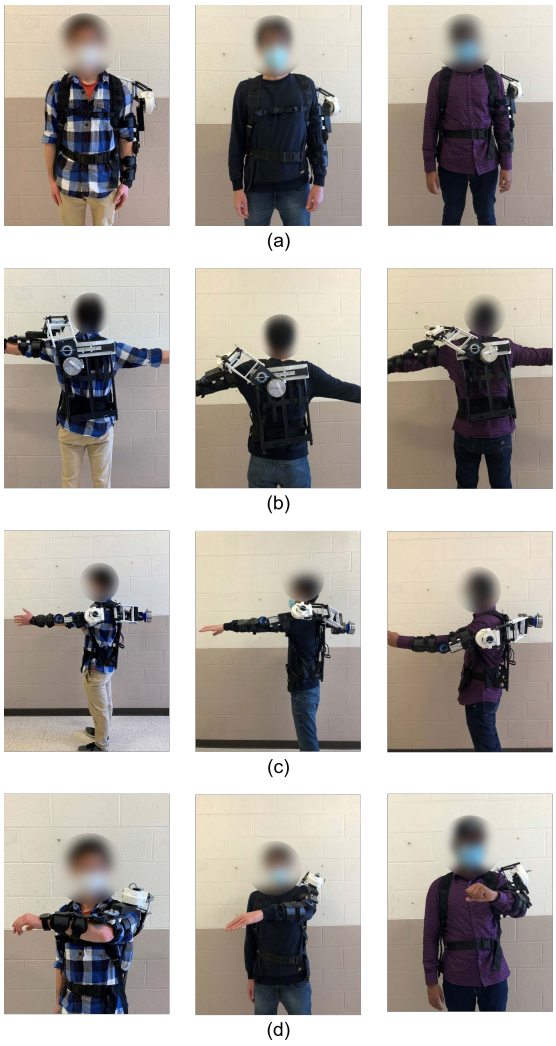

Fig. 10. Three subjects wearing the rehabilitation device in a (a) relaxed position, (b) performing a T-pose, (c) performing shoulder flexion, and (d) reaching across their bodies

the torque transfer from the motor to the user's arm in different configurations and frequencies. These features along with backdrivability and counterweight support seek to improve the exoskeleton's ergonomics. Comprehensive experiments validated the ability of the system to generate arm swing and its wide workspace. While we presented a proof-of-concept prototype, future work will focus on developing a more robust prototype using the presented mechanism and evaluating its performance using individuals post-stroke.

TABLE IV

RANGE OF MOTION WHILE WEARING THE REHABILITATION DEVICE.

Movement	Human	Rehabilitation Device	Coverage
Flexion	170°	144.89°	85.23%
Extension	-60°	-50.39°	83.99%
Abduction	120°	171.5°	100.00%
Adduction	-20°	-64.81°	100.00%
External	90°	30.15°	33.50%
Internal	-60°	-85.91°	100.00%

REFERENCES

[1] B. Hejrati, S. Chesebrough, K. B. Foreman, J. J. Abbott, and A. S. Merryweather, "Comprehensive quantitative investigation of arm swing during walking at various speed and surface slope conditions," *Human movement science*, vol. 49, pp. 104–115, 2016.

[2] O. R. Barnes, B. Hejrati, and J. J. Abbott, "An underactuated wearable arm-swing rehabilitator for gait training," in *2015 IEEE international conference on robotics and automation (ICRA)*. IEEE, 2015, pp. 4998–5003.

[3] D. P. Ferris, H. J. Huang, and P.-C. Kao, "Moving the arms to activate the legs," *Exercise and sport sciences reviews*, vol. 34, no. 3, pp. 113–120, 2006.

[4] B. Hejrati, A. S. Merryweather, and J. J. Abbott, "Generating arm-swing trajectories in real-time using a data-driven model for gait rehabilitation with self-selected speed," *IEEE Transactions on Neural Systems and Rehabilitation Engineering*, vol. 26, no. 1, pp. 115–124, 2017.

[5] D. de Kam, J. Duysens, and V. Dietz, "Do we need allowing arm movements for rehabilitation of gait?" pp. 959–962, 2013.

[6] N. J. Tester, D. R. Howland, K. V. Day, S. P. Suter, A. Cantrell, and A. L. Behrman, "Device use, locomotor training and the presence of arm swing during treadmill walking after spinal cord injury," *Spinal Cord*, vol. 11(49), pp. 451–6, 2011.

[7] E. Trigili, S. Crea, M. Moisè, A. Baldoni, M. Cempini, G. Ercolini, D. Marconi, F. Posteraro, M. C. Carrozza, and N. Vitiello, "Design and experimental characterization of a shoulder-elbow exoskeleton with compliant joints for post-stroke rehabilitation," *IEEE/ASME Transactions on Mechatronics*, vol. 24, no. 4, pp. 1485–1496, 2019.

[8] S. Buccelli, F. Tessari, F. Fanin, L. De Guglielmo, G. Capitta, C. Piezzo, A. Bruschi, F. Van Son, S. Scarpetta, A. Succi *et al.*, "A gravity-compensated upper-limb exoskeleton for functional rehabilitation of the shoulder complex," *Applied Sciences*, vol. 12, no. 7, p. 3364, 2022.

[9] M. A. Noghani, M. T. Hossain, and B. Hejrati, "Modulation of arm swing frequency and gait using rhythmic tactile feedback," *IEEE Transactions on Neural Systems and Rehabilitation Engineering*, vol. 31, pp. 1542–1553, 2023.

[10] S. Mainka, A. Schroll, E. Warmerdam, F. Gandor, W. Maetzler, and G. Ebersbach, "The power of musification: Sensor-based music feedback improves arm swing in parkinson's disease," *Movement Disorders Clinical Practice*, vol. 8, no. 8, pp. 1240–1247, 2021.

[11] S. Christensen and S. Bai, "Kinematic analysis and design of a novel shoulder exoskeleton using a double parallelogram linkage," *Journal of Mechanisms and Robotics*, vol. 10, no. 4, 2018.

[12] H.-C. Hsieh, D.-F. Chen, L. Chien, and C.-C. Lan, "Design of a parallel actuated exoskeleton for adaptive and safe robotic shoulder rehabilitation," *IEEE/ASME Transactions on Mechatronics*, vol. 22, no. 5, pp. 2034–2045, 2017.

[13] J. Hunt, H. Lee, and P. Artemiadis, "A novel shoulder exoskeleton robot using parallel actuation and a passive slip interface," *Journal of Mechanisms and Robotics*, vol. 9, no. 1, 2017.

[14] S. Roderick, M. Liszka, and C. Carignan, "Design of an arm exoskeleton with scapula motion for shoulder rehabilitation," in *ICAR'05. Proceedings., 12th International Conference on Advanced Robotics, 2005.* IEEE, 2005, pp. 524–531.

[15] L. Tiseni, M. Xiloyannis, D. Chiaradia, N. Lotti, M. Solazzi, H. Van der Kooij, A. Frisoli, and L. Masia, "On the edge between soft and rigid: an assistive shoulder exoskeleton with hyper-redundant kinematics," in *2019 IEEE 16th International Conference on Rehabilitation Robotics (ICORR)*. IEEE, 2019, pp. 618–624.

[16] C. O'Neill, T. Proietti, K. Nuckols, M. E. Clarke, C. J. Hohimer, A. Cloutier, D. J. Lin, and C. J. Walsh, "Inflatable soft wearable robot for reducing therapist fatigue during upper extremity rehabilitation in severe stroke," *IEEE Robotics and Automation Letters*, vol. 5, no. 3, pp. 3899–3906, 2020.

[17] M. Jones, C. Bouffard, and B. Hejrati, "A shoulder mechanism for assisting upper arm function with distally located actuators," in *2019 41st Annual International Conference of the IEEE Engineering in Medicine and Biology Society (EMBC)*. IEEE, 2019, pp. 6233–6236.

[18] P. De Leva, "Adjustments to zatsiorsky-seluyanov's segment inertia parameters," *Journal of biomechanics*, vol. 29, no. 9, pp. 1223–1230, 1996.

[19] S. Chesebrough, B. Hejrati, and J. Hollerbach, "The treadport: natural gait on a treadmill," *Human factors*, vol. 61, no. 5, pp. 736–748, 2019.